J. Fluid Mech. (1978), *vol.* 89, *part* 2, *pp.* 223–240
Printed in Great Britain

Bubbly flow model for the dynamic characteristics of cavitating pumps

By CHRISTOPHER BRENNEN

Division of Engineering and Applied Science,
California Institute of Technology, Pasadena

(Received 13 June 1977)

This paper is concerned with understanding the dynamic behaviour of cavitating hydraulic machines during unsteady or transient operation. The linear transfer matrices which relate the small fluctuating pressures and mass flow rates at inlet and discharge are functions not only of the frequency but also of the mean operating state of the machine, especially the degree of cavitation. The recent experimental transfer matrices obtained by Ng & Brennen (1978) for some axial flow pumps revealed some dynamic characteristics which were unaccounted for by any existing theoretical analysis; their visual observations suggested that the bubbly cavitating flow in the blade passages could be responsible for these effects.

A theoretical model of the dynamic response of this bubbly blade-passage flow is described in the present paper. Void-fraction fluctuations in this flow result not only from pressure fluctuations but also because the fluctuating angle of attack causes fluctuations in the rate of production of bubbles near the leading edge. The latter causes kinematic waves which interact through the boundary conditions with the dynamic waves caused by pressure fluctuation. The resulting theoretical transfer functions which result are in good qualitative agreement with the experiments; with appropriate choices of two parameters (the practical values of which are difficult to assess) good quantitative agreement is also obtained. The theoretical model also provides one possible explanation of the observation that the pump changes from an essentially passive dynamic element in the absence of cavitation to a progressively more active element as the extent of cavitation increases.

1. Introduction

The purpose of this paper is to present an approximate theoretical model for the dynamic characteristics of cavitating hydraulic machines. It is motivated by a desire to understand some of the fundamental dynamic phenomena manifest in the recent experimental dynamic transfer functions obtained by Ng & Brennen (1978; see also Ng 1976; Ng, Brennen & Acosta 1976) for cavitating (and non-cavitating) axial inducer pumps. Those experimental results were presented in the form of dynamic transfer matrices $[ZP]$ relating the linearized fluctuating pressures and mass flow rates at the inlet to and discharge from the hydraulic machine. In particular, $[ZP]$ was defined as

$$\begin{Bmatrix} \tilde{h}_2 - \tilde{h}_1 \\ \tilde{m}_2 - \tilde{m}_1 \end{Bmatrix} = \begin{bmatrix} ZP_{11} & ZP_{12} \\ ZP_{21} & ZP_{22} \end{bmatrix} \begin{Bmatrix} \tilde{h}_1 \\ \tilde{m}_1 \end{Bmatrix}, \tag{1}$$

where the subscripts 1 and 2 refer to conditions at the inlet and discharge and $\tilde{h}$ and $\tilde{m}$ are the non-dimensional oscillating total pressure and mass flow rate. The total pressure, which is defined as the sum of the local static pressure and the local velocity head based on the instantaneous velocity, is made dimensionless by dividing by $\frac{1}{2}\rho_L U_T^2$, where ρ_L is the liquid density and U_T is the speed of the impeller tip. The mass flow rate is made dimensionless by dividing by $\rho_L U_T A_i$, where A_i is the cross-sectional area of the flow at the inlet plane of the impeller.

In general $\tilde{h}$ and $\tilde{m}$ are complex in order to represent the phase differences between the oscillating quantities; thus, in general, $[ZP]$ is complex. Furthermore $[ZP]$ is a function not only of the frequency Ω but also of the mean operating state of the hydraulic machine, including the extent of cavitation.

The quantity $-ZP_{12}$ represents the non-dimensional impedance of the machine and is comprised of resistive and inertial components; at low frequency the resistance approaches a value which is simply given by the slope of the steady-state characteristic of head rise *vs.* flow rate. The quantities ZP_{21} and ZP_{22}, which describe the difference between the instantaneous inlet and discharge flow rates, would be expected to be zero *either* (i) at low frequency *or* (ii) in the absence of cavitation or some other second, gaseous component within the flow (neglecting the liquid and structural compressibility of the machine). Furthermore the element ZP_{11} should also be zero in the absence of cavitation (or a second, gaseous component) since under such circumstances the head rise does not depend upon the absolute level of the inlet or discharge pressure. In the presence of cavitation at low frequencies one might anticipate that ZP_{11} should approach a value given by the slope of the steady-state characteristic of head rise *vs.* cavitation number. The experiments of Ng & Brennen (1978) were carried out to investigate how each of the elements varied with the degree of cavitation and with the frequency for some typical axial flow pumps. In the next section we shall discuss the experimental transfer matrices and present some further analysis which was performed for the purpose of more readily comparing those data with the theoretical model.

The theoretical model presented in this paper was suggested and guided by visual observations of the cavitating flows made during the experiments reported in Ng & Brennen (1978). In an actual pump impeller cavitation is produced at or near the leading edges of the blades and can take a number of forms (Brennen 1973). Most often in nominally steady flows it takes the form of a train of vapour bubbles (which may also contain some air) on the suction sides of the blades; these are convected through the blade passage, finally collapsing when they move into regions of higher pressure. Bubbles which have a similar subsequent history are often formed in the tip vortices at the leading edges of the blade tips. In the more advanced stages of cavitation fixed cavities or vapour-filled wakes may form on the suction sides of the blades; however, such fully developed cavities are normally accompanied by a great deal of bubbly cavitation and also degenerate into the bubbly form near the ends of the fixed cavities. We include here as figure 1 (plate 1) a high-speed photograph of cavitation taken during one of the experiments of Ng & Brennen (1978); this was taken under mean flow conditions of extensive cavitation and shows the bubbly form of the cavitation in the blade passages of one of the inducers. High-speed motion pictures of the same kinds of flow revealed observable fluctuations in this pattern of cavitation under oscillatory dynamic conditions. Thus the central element of the theoretical model

whose development begins in § 3 deals with the dynamic response of this bubbly-passage flow.

Previous theoretical attempts to simulate the dynamic characteristics of hydraulic machines have usually been made in the absence of complete and detailed experimental data. Though this is particularly true in the cavitating case, the dynamic data for non-cavitating flows are also limited, the work of Anderson, Blade & Stevens (1971) being one exception. Fanelli (1972) has been one of the leaders in developing theoretical methods for the analysis of the characteristics of non-cavitating hydraulic machines. Early attempts to construct theoretical models for cavitating pumps (e.g. Rubin 1966; Wagner 1971; Vaage, Fidler & Zehnle 1972; Farrel & Fenwick 1973; Brennen & Acosta 1973; Brennen 1973) used the slopes of the steady-state characteristics of head rise *vs.* flow rate and cavitation number plus some added 'cavitation compliance' C, so that $ZP_{21} = -i\Omega C$. Brennen & Acosta (1976) first pointed out that cavitation would also lead to a non-zero value of ZP_{22} like $-i\Omega M$ at low frequencies, where M, the 'mass flow gain factor', arose because of the variation in the volume of cavitation with the angle of attack at the leading edges of the blades.

Most of this later work concentrated on the contributions of fully developed and attached blade cavities to both C and M. The contribution of the predominant bubbly form of cavitation to the dynamic characteristics has been relatively neglected though there has been some preliminary work on the dynamic response of cavitating streams of bubbles (Brennen 1973). The present paper represents an attempt to rectify this earlier neglect.

Finally it is worth noting that though we concentrate here on applications to cavitating flows, it should be apparent that the model could quite readily be adjusted and used to study the dynamics of other kinds of two-phase and two-component flows in either pumps or turbines. In particular, the dynamic problems in the operation of multiphase pumping referred to by Runstadler (1976) are closely related to the kinds of phenomena investigated in this paper.

2. Experimental transfer matrices

In the absence of cavitation Ng & Brennen (1978) found as expected that ZP_{11}, ZP_{21} and ZP_{22} were all effectively zero, the liquid and structural compressibility within the pump being negligible. The impedances (given by $-ZP_{12}$) which were obtained tended towards the expected resistive and inertial components at low frequency. However, as the non-dimensional frequency increased towards the highest investigated (0·5) the resistance first increased and then decreased and the inertia decreased (for details see Ng & Brennen 1978). Similar frequency-dependent resistances and inertias had also been seen in the non-cavitating performance of a centrifugal pump by Anderson *et al.* (1971).

The situation was considerably different when even a quite modest amount of cavitation was present. As the degree of cavitation was increased ZP_{11}, ZP_{21} and ZP_{22} all became increasingly non-zero and ZP_{12} deviated from its non-cavitating form. Typical experimental results were presented in Ng & Brennen (1978) for a 7·58 cm diameter axial inducer which is a model of the low pressure oxidizer pump in the Space Shuttle main engine (Impeller IV). The qualitative characteristics of the transfer matrices for another impeller were quite similar; we shall concentrate here on Impeller

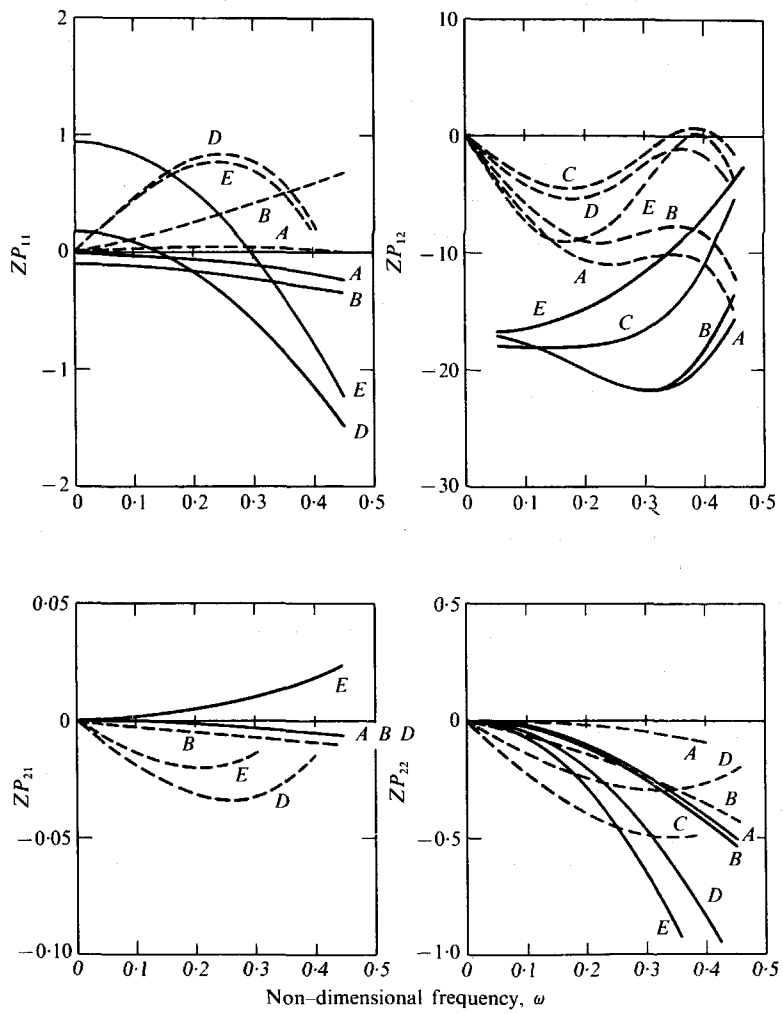

FIGURE 2. Polynomial curve fitting to experimental pump transfer matrices $[ZP]$ obtained for Impeller IV at $\phi = 0{\cdot}070$ and a rotational speed of 9000 r.p.m. (Ng & Brennen 1978). The real and imaginary parts of the matrix elements are presented as functions of frequency by solid and dashed lines respectively. The letters A to E are the designations used by Ng & Brennen to denote matrices taken at five progressively diminishing cavitation numbers σ as follows: (A) 0·508; (B) 0·114; (C) 0·046; (D) 0·040; (E) 0·023.

IV, for which a larger number of matrices were obtained (for fourteen mean operating states, each at seven different frequencies). The mean operating state was described by the flow coefficient ϕ, defined as U_A/U_T where U_A and U_T are respectively the average mean flow velocity at the leading edge of the inducer and the tip velocity of the inducer, and by the cavitation number σ, defined as $(p_1^* - p_v^*)/\frac{1}{2}\rho_L U_T^2$, where p_1^* and p_v^* are respectively the mean pressure upstream of the inducer and the vapour pressure. The dimensionless frequency ω was defined as $\Omega h/U_T$, where h is the blade-tip spacing ($= 2\pi R/N$, where R is the blade-tip radius, N the number of blades). The transfer matrices for Impeller IV were obtained at $\phi = 0{\cdot}070$ (7 different σ's at a rotation speed of 9000 r.p.m., 3 different σ's at 12000 r.p.m.) and at $\phi = 0{\cdot}076$

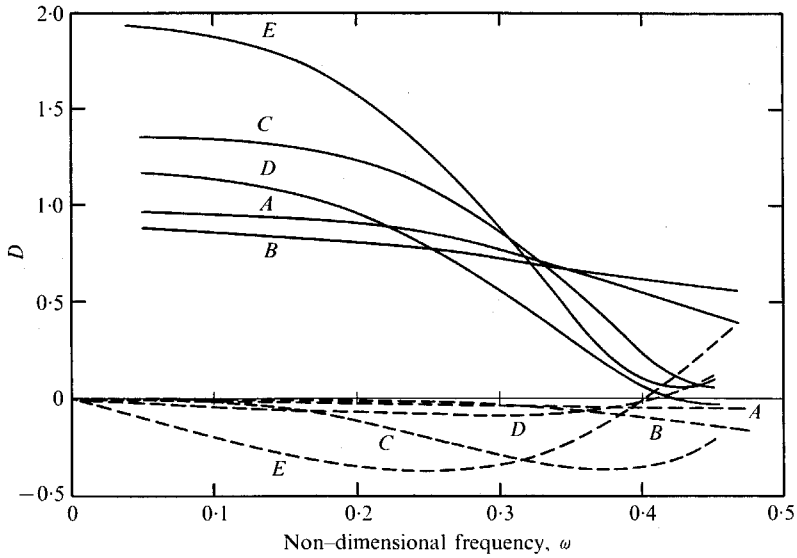

FIGURE 3. The determinants D for the matrices (plus the unit matrix) in figure 2; solid and dashed lines again represent real and imaginary parts respectively.

(4 different σ's at 9000 r.p.m.). Subsequently we have fitted (using a least-squares procedure) both the real and the imaginary parts of the four $[ZP]$ elements for each mean operating state (ϕ, σ) to simple polynomials in $i\omega$ of the form

$$ZP_{IJ} = \sum_{N=0}^{N_{IJ}} a_{NIJ}(i\omega)^N, \tag{2}$$

where N_{11}, N_{21}, $N_{22} = 3$ and $N_{12} = 5$. The higher order for ZP_{12} represents an attempt to extract a little more of the evident detail in the frequency-dependent resistance $-a_{012}+\omega^2 a_{212}-\omega^4 a_{412}$ and inertia $-a_{112}+\omega^2 a_{312}-\omega^4 a_{512}$ comprising the impedance. Quasi-static considerations of continuity of mass (e.g. Brennen & Acosta 1976) demand that a_{021} and a_{022} should be zero, thus they were set at these values prior to the fitting procedure. Preliminary examination (see Ng & Brennen 1978) of the remaining non-zero coefficients (particularly the compliance $-a_{121}$ and the mass flow gain factor $-a_{122}$) and their variation with σ strongly suggested a dependence like $\sigma^{-\frac{1}{2}}$ and σ^{-1} for these coefficients.

The results of this fitting procedure for the cases in which $\phi = 0{\cdot}070$ are presented in figure 2 in the form of the variation of each of the four elements with frequency for various cavitation numbers. The real and imaginary parts are displayed as solid and dashed lines respectively. The real and imaginary parts of the determinant

$$D = (ZP_{11}+1)\,(ZP_{22}+1) - ZP_{12}ZP_{22} \tag{3}$$

are presented similarly in figure 3. All of the qualitative characteristics of these curves are also evident in the basic data as can be determined by comparison with the three transfer functions presented in Ng & Brennen (1978). Further discussion of the data in figures 2 and 3 will accompany the comparison with figures 5 and 6.

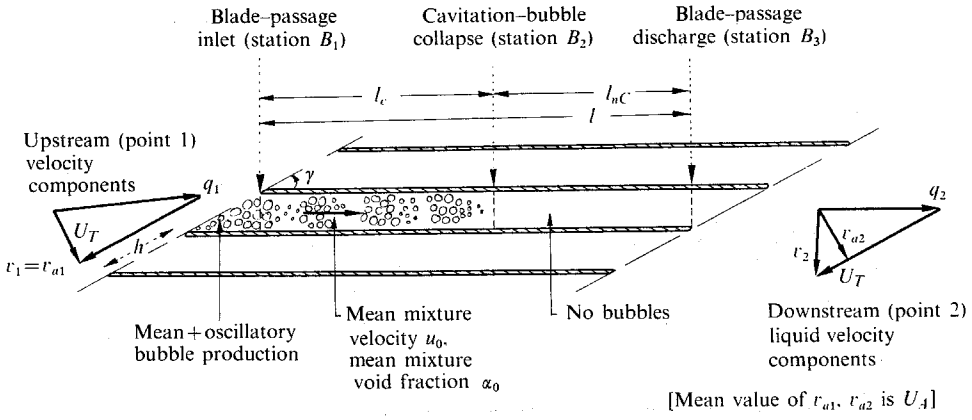

FIGURE 4. Schematic diagram of the cascade used in the bubbly blade-passage flow model of pump dynamics.

3. Cavitating or two-phase inducer model

The purpose of this section is to do the groundwork for the later examination of the dynamic consequences of bubbly flow in the blade passages of a pump impeller. We shall assume that the flow through the impeller has no radial component and examine the resulting cascade flow indicated in figure 4; this figure depicts the basic hydrodynamic model which will be investigated. The flow of pure liquid upstream of the inducer is indicated by the upstream velocity triangle; here v_1 is the absolute liquid velocity (assumed purely axial and therefore equal to its axial component v_{a1}) and q_1 is the velocity relative to the inducer blades, whose velocity is denoted by U_T. To simplify the dynamic problem it will be assumed that the inducer velocity U_T is a constant and does not oscillate (in many practical situations this is indeed the case). The velocities q_1 and v_{a1} have mean (time-averaged) components upon which are superimposed small oscillatory components; for convenience the mean value of v_{a1} is denoted by U_A, so that the flow coefficient ϕ of the mean flow is U_A/U_T. Other quantities at this upstream point 1 are designated by the single subscript 1.

Clearly the dynamic response of the kinds of cavitating flow described in § 1 is a very complex matter indeed. In this paper we shall construct a rather gross model of the cavitation, but one which is at least amenable to dynamic analysis. The variations in the flow across the blade passage will be smeared out so that the analysis of the events in the passage is purely one-dimensional and quantities vary only with x, the co-ordinate measured along the passage from the blade-passage entrance. The point at which the bubbles collapse is denoted by $x = l_c$ (figure 4); downstream of this point it is assumed that the passage contains only liquid, the blade-passage discharge being located at $x = l$.

The volume of bubbles in the blade passage in any steady cavitating flow is primarily a function of the cavitation number σ and angle of attack β. Though, in practice, there are also Reynolds number effects, Weber number effects and often strong thermal effects (Brennen 1973), we shall neglect these for the purposes of this paper. We shall denote the time- and space-averaged mean void fraction of the bubbles in the region $0 < x < l_c$ by α_0, and assume that there is no slip velocity between the

phases in this region. If the blade thickness is neglected (though its effects could readily be included) it follows from continuity that the mean velocity in the blade passage is $u_0 = U_A/(1-\alpha_0)\sin\gamma$ in $0 < x < l_c$ and $U_A/\sin\gamma$ in $l_c < x < l$. To compute results we shall need to choose representative values of α_0; these will clearly increase with decreasing σ. Apart from direct observation, which is difficult, an estimate of the effective values of α_0 is suggested by the work of Stripling & Acosta (1962). They demonstrated that the additional inducer head loss associated with cavitation could be attributed in large measure to the lack of efficient pressure recovery in the flow near the cavity collapse region. That is to say, the mixing losses in this region dissipate any potential pressure rise accompanying the reduction in velocity from the value $U_A/(1-\alpha_0)\sin\gamma$ to $U_A/\sin\gamma$. If the head coefficient ψ is defined as the total head rise across the pump divided by ρU_T^2, then the reduction $\Delta\psi$ in this value associated with the cavitation will be of order

$$\Delta\psi = \alpha_0(2-\alpha_0)\,\phi^2/2(1-\alpha_0)^2\sin^2\gamma. \tag{4}$$

With this functional relation $\Delta\psi(\alpha_0, \phi)$ and given the cavitation performance of an inducer in the form $\Delta\psi(\sigma, \phi)$ one can clearly deduce some rough estimate of the relation between α_0 and σ. For example, the steady-state cavitation performance data for Impeller IV (see Ng & Brennen 1977) yielded values of α_0 of about 0·16, 0·10 and 0·02 at $\sigma = 0{\cdot}02$, 0·03 and 0·045 respectively. On this basis we can make a reasonable estimate of the effective value of α_0 at a given cavitation number.

As the upstream flow oscillates, this produces a fluctuation in the angle of attack β. This will produce a fluctuation in the number and volume of bubbles generated at the leading edge per unit time. Furthermore, we shall assume that this inhomogeneity in the void fraction or mixture density is convected through the blade passage at the mixture velocity u_0 (figure 4). This leads to fluctuating terms like $\tilde{\alpha}_A \exp(i\Omega t - i\Omega x/u_0)$ in the void fraction or $-\rho_L\tilde{\alpha}_A \exp(i\Omega t - i\Omega x/u_0)$ in the mixture density in the blade passage (t is time). We shall assume that the amplitude $\tilde{\alpha}_A$ is proportional to the amplitude of the angle of attack fluctuation and therefore proportional to the amplitude of the upstream mass flow rate fluctuation $\tilde{m}_1$ according to

$$\tilde{\alpha}_A = -M^*\tilde{m}_1. \tag{5}$$

We shall see that the factor of proportionality M^* is analogous in its dynamic effect to the mass flow gain factor derived previously for fully developed leading-edge blade cavities (Brennen & Acosta 1976).

In the region $0 < x < l_c$ of the blade passage the pressure $p(x)$, mixture density $\rho(x)$, void fraction $\alpha(x)$ and mixture velocity $u(x)$ are divided into their mean and fluctuating components according to the notation

$$\left.\begin{aligned} p(x) &= p_0 + \tilde{p}(x)\,e^{i\Omega t}, \quad \rho(x) = \rho_0 + \tilde{\rho}(x)\,e^{i\Omega t}, \\ \alpha(x) &= \alpha_0 + \tilde{\alpha}(x)\,e^{i\Omega t}, \quad u(x) = u_0 + \tilde{u}(x)\,e^{i\Omega t}, \end{aligned}\right\} \tag{6}$$

where p_0, $\rho_0 = \rho_L(1-\alpha_0)$, α_0 and u_0 are assumed independent of x. The *local* mixture density $\tilde{\rho}(x) = -\rho_L\tilde{\alpha}(x)$ or void fraction will also be a function of the local pressure $\tilde{p}(x)$. To represent this we require a compressibility K^* for the mixture. The compressibility of a gas/liquid mixture, namely $\alpha_0(1-\alpha_0)\rho_L/p$, where p is the pressure, is *not* appropriate since cavitation bubbles have a much greater compressibility. However, some earlier work on the dynamics of streams of cavitating bubbles

(Brennen 1973) suggests that to a first approximation we might still consider the cavitating bubble/liquid mixture to have some compressibility K^*, which will be assumed uniform. If this fluctuation with pressure is superimposed on the inhomogeneity described earlier the mixture density is then given by

$$\tilde{\rho}(x) = \rho_L M^* \tilde{m}_1 \exp(-i\Omega x/u_0) + K^* \tilde{p}(x). \tag{7}$$

It also follows that if the cross-sectional area of the blade passage is A_{BP} (assumed constant) then the mean mass flow of liquid is $\rho_0 u_0 A_{BP}$ and the fluctuating mass flow of liquid is $A_{BP}\{\rho_0 \tilde{u}(x) + u_0 \tilde{\rho}(x)\}$. It is convenient for the purpose of the analysis of the blade-passage dynamics to define the non-dimensional mass flow fluctuation amplitude $\tilde{m}(x)$ as a fraction of the mean mass flow (note that this differs by a factor ϕ from the dimensionless pump inlet and discharge mass flow rates $\tilde{m}_1$ and $\tilde{m}_2$) so that

$$\tilde{m}(x) = \frac{\tilde{u}(x)}{u_0} + \frac{M^*}{1-\alpha_0} \tilde{m}_1 \exp\left(-i\frac{\Omega x}{u_0}\right) + \frac{K^*}{\rho_0} \tilde{p}(x). \tag{8}$$

The values of $\tilde{m}$ at $x = 0$ and $x = l_c$ must clearly be equal to the fractional amplitudes of the mass flow rate fluctuation far upstream and far downstream of the pump respectively, so that

$$\tilde{m}(0) = \tilde{m}_1/\phi, \quad \tilde{m}(l_c) = \tilde{m}(l) = \tilde{m}_2/\phi. \tag{9}$$

4. Blade-passage dynamics

We are now in a position to discuss the dynamic behaviour of the flow in the blade passage. Since this is assumed to have a constant cross-sectional area continuity of mass requires that

$$\frac{\partial \rho}{\partial t} + \frac{\partial}{\partial x}(\rho u) = 0, \tag{10}$$

or in terms of the fluctuating quantities defined by the (6),

$$i\Omega\tilde{\rho} + \rho_0 \frac{\partial \tilde{u}}{\partial x} + u_0 \frac{\partial \tilde{\rho}}{\partial x} = 0. \tag{11}$$

Furthermore, the equation of motion governing these fluctuating quantities is

$$\frac{\partial \tilde{p}}{\partial x} + i\Omega\rho_0 \tilde{u} + \rho_0 u_0 \frac{\partial \tilde{u}}{\partial x} = -\rho_L u_0 f \tilde{u}, \tag{12}$$

where we have inserted a characteristic frictional term on the right-hand side to simulate the frictional resistance in the blade passage, f being a friction coefficient (actually the conventional friction factor divided by the hydraulic radius). Substituting (7) into (11) we obtain

$$i\Omega K^* \tilde{p} + u_0 K^* \frac{\partial \tilde{p}}{\partial x} + \rho_0 \frac{\partial \tilde{u}}{\partial x} = 0. \tag{13}$$

The solution of (12) and (13) for $\tilde{p}(x)$ and $\tilde{u}(x)$ yields

$$\tilde{p}(x) = \rho_0 u_0^2 [\xi_1 G \exp(\eta_1 x/l_c) + \xi_2 H \exp(\eta_2 x/l_c)], \tag{14}$$

$$\tilde{m}(x) = G\exp(\eta_1 x/l_c) + H\exp(\eta_2 x/l_c) + M\tilde{m}(0)\exp(-i\Omega x/u_0), \tag{15}$$

where $M = M^*\phi/(1-\alpha_0)$ and (8) and (9) have been used. Here G and H are constants and η_1 and η_2 are the solutions of the dispersion relation

$$\eta^2 = K\phi\lambda(\eta + i\Omega l_c/u_0)\,(\eta + i\Omega l_c/u_0 + f l_c(1-\alpha_0)), \tag{16}$$

where for later convenience we have defined $K \equiv K^* U_T^2$ and the factor $\phi/(1-\alpha_0)^2 \sin^2\gamma$ is denoted by λ. Furthermore in (14)

$$\xi_{1,2} = (i/\Omega l_c K^* u_0)\,\eta_{1,2}. \tag{17}$$

It follows from (14) and (15) that the pressures and fractional mass flow rates at the limits of the bubbly region are related by

$$\begin{Bmatrix} \tilde{p}(l_c) - \tilde{p}(0) \\ \tilde{m}(l_c) - \tilde{m}(0) \end{Bmatrix} = \begin{bmatrix} ZB_{11} & \frac{1}{2}\rho_0 u_0^2 ZB_{12} \\ 2ZB_{21}/\rho_0 u_0^2 & ZB_{22} \end{bmatrix} \begin{Bmatrix} \tilde{p}(0) \\ \tilde{m}(0) \end{Bmatrix}, \tag{18}$$

where
$$ZB_{11} = -1 + [\eta_1 \exp(\eta_1) - \eta_2 \exp(\eta_2)]/(\eta_1 - \eta_2), \tag{19}$$

$$ZB_{12} = -\frac{2(1-M)}{(1-K\phi\lambda)}\left(i\frac{\Omega l_c}{u_0} + f l_c(1-\alpha_0)\right)[\exp(\eta_1) - \exp(\eta_2)]/(\eta_1 - \eta_2), \tag{20}$$

$$ZB_{21} = -\frac{i\Omega l_c K\phi\lambda}{2u_0}[\exp(\eta_1) - \exp(\eta_2)]/(\eta_1 - \eta_2), \tag{21}$$

$$ZB_{22} = -1 + Me^{-i\Omega l_c/u_0} + (1-M)[\eta_1 \exp(\eta_2) - \eta_2 \exp(\eta_1)]/(\eta_1 - \eta_2). \tag{22}$$

These elements then comprise the transfer function for the bubbly region of flow. Though further manipulation is necessary (see below) to obtain the transfer function for the pump, it is nevertheless worthwhile examining the above elements in order to identify the physical components which they imply. If η_1, $\eta_2 \ll 1$ ($K\lambda \ll 1$ and $\Omega l_c/u_0 \ll 1$) then the elements ZB become

$$ZB_{11} \approx K\phi\lambda\left\{2i\frac{\Omega l_c}{u_0} + f l_c(1-\alpha_0)\right\}, \quad ZB_{12} \approx -2(1-M)\left(\frac{i\Omega l_c}{u_0} + f l_c(1-\alpha_0)\right), \tag{23), (24}$$

$$ZB_{21} \approx -i\left(\frac{\Omega l_c}{u_0}\right)\frac{K\phi\lambda}{2}, \quad ZB_{22} \approx -i\left(\frac{\Omega l_c}{u_0}\right)M. \tag{25), (26}$$

Comparing these with the quasi-steady analysis of pump dynamics (Brennen & Acosta 1976; Ng & Brennen 1978), we see that ZB_{12} contains inertial and resistive terms $O(i\Omega)$ and $O(1)$ respectively, ZB_{21} contains the expected compliance term and ZB_{22} contains the expected mass flow gain factor.

Finally for future purposes we also note that the determinant D of $[ZB] + [I]$, where $[I]$ is the unit matrix, is

$$D = \frac{\eta_1 \exp(\eta_1) - \eta_2 \exp(\eta_2)}{\eta_1 - \eta_2} M \exp(-i\Omega l_c/u_0) + (1-M)\exp(\eta_1 + \eta_2), \tag{27}$$

which for small $\Omega l_c/u_0$ and $K\lambda$ reduces to

$$D \approx (1 - i\Omega l_c M/u_0)(1 + 2i\Omega l_c K\phi\lambda/u_0 + f l_c K\phi\lambda). \tag{28}$$

5. Pump transfer function

In order to construct the pump transfer function we must now relate the pressures and mass flow rates at $x = 0$ and $x = l_c$ to their values upstream and downstream of the cascade. The relations between the mass flow rates have already been described in (9); it remains to relate the pressures.

In nominally steady flow it is conventional to define pump characteristics in terms of total-head quantities rather than the static pressure upstream and downstream of the pump. In the present dynamic study we therefore define a dynamic total pressure quantity H_i which is the sum of the instantaneous pressure and the instantaneous dynamic contribution either upstream ($i = 1$) or downstream of the pump ($i = 2$). This is then divided into a mean component H_{0i}, and an oscillatory component $\tilde{H}_i$, according to

$$H_i = H_{0i} + \tilde{H}_i e^{i\Omega t}. \tag{29}$$

Furthermore we non-dimensionalize $\tilde{H}_i$ by dividing by $\frac{1}{2}\rho_L U_T^2$ to obtain the dimensionless dynamic total pressure $\tilde{h}_i$. It follows from linearization that

$$\tilde{h}_i = \tilde{p}_i/(\tfrac{1}{2}\rho_L U_T^2) + 2\phi\tilde{m}_i, \tag{30}$$

where $\tilde{p}_i$ is the oscillatory static pressure.

Now if we assume that the fluid velocity relative to the blades is parallel to the blades at the entrance $x = 0$ to the blade passage (figure 4) it follows that

$$H_1 + (\partial\phi/\partial t)_1 - (\partial\phi/\partial t)_{x=0} = p(0) + \tfrac{1}{2}\rho_L\{u(0)\}^2. \tag{31}$$

The $\partial\phi/\partial t$ terms represent a pressure difference due to the inertia of the mass of fluid between the point 1 and the blade-passage entrance (or leading edge of the pump blades). The experimental data (Ng & Brennen 1978) are usually given in terms of an H_1, from which this inertia contribution has been removed; thus we may delete the $\partial\phi/\partial t$ terms. Using continuity, it follows that the linearized perturbation quantities are related by

$$\tilde{p}(0) = \tfrac{1}{2}\rho_L U_T^2\{\tilde{h}_1 - 2\phi\tilde{m}_1/(1-\alpha_0)^2\sin^2\gamma\} \tag{32}$$

and with $\tilde{m}(0) = \tilde{m}_1/\phi$ this completes the necessary link with the blade-passage flow on the inlet side.

Downstream of the bubbly flow we must first relate $\tilde{p}(l_c)$ to $\tilde{p}(l)$ at the blade-passage discharge. We retain the same friction coefficient for $l_c < x < l$ as was used in $0 < x < l_c$. Clearly this is not necessary and it is only done here for simplicity. Then the relation between $\tilde{p}(l_c)$ and $\tilde{p}(l)$ can be obtained either by constructing its inertial and resistive parts or by taking the appropriate limits of the analysis in the last section and applying it to the region $l_c < x < l$:

$$\tilde{p}(l) = \tilde{p}(l_c) - \frac{\rho_L(l-l_c)\,U_A^2}{\sin^2\gamma}\left\{\frac{i\Omega\sin\gamma}{U_A} + f\right\}\tilde{m}(l). \tag{33}$$

Finally $\tilde{p}(l)$ may be related to the downstream dynamic total pressure $\tilde{h}_2$ in a manner analogous to that by which the relations at the inlet were obtained. Hence

$$\tilde{p}(l) = \tfrac{1}{2}\rho_L U_T^2\{\tilde{h}_2 + 2\tilde{m}_2\cot\gamma - 2\phi\tilde{m}_2\,\mathrm{cosec}^2\gamma\}. \tag{34}$$

The second term in the braces in (34) is most important; it is analogous to the usual theoretical slope of the head rise *vs.* flow curve for a pump [this may be seen by setting

$\tilde{p}(0) = \tilde{p}(l)$ and $\tilde{m}_1 = \tilde{m}_2$ and subtracting (32) from (34)]. The actual experimental slope of this curve is modified by a difference between the pressures $\tilde{p}(0)$ and $\tilde{p}(l)$ due to the many kinds of loss which occur in an actual axial flow pump. These loss terms are represented here by the friction coefficient f included in the blade-passage analysis.

It remains only to use (32)–(34) in order to construct the pump transfer function $[ZP]$ from the transfer function $[ZB]$. The resulting elements of $[ZP]$ can then be written in terms of the following variables:

(i) The blade angle γ.

(ii) The geometric ratio $\tau = l\sin\gamma/h$ of the axial inducer length to the blade-tip spacing.

(iii) The flow coefficient ϕ.

(iv) The usual, dimensionless frequency for pump dynamics $\omega = \Omega h/U_T$.

(v) A blade-passage resistance parameter $F = fl\phi/\sin^2\gamma$. In the results which follow this was simply chosen such that the total pump resistance (or magnitude of the real part of ZP_{12}) matched the experimental data for quasi-steady or mean flow performance.

(vi) The fractional length of the bubbly region $\epsilon = l_c/l$. In practice this is in turn a function of ϕ and the cavitation number σ.

(vii) The mean void fraction α_0. Values could be determined as indicated in § 3.

(viii) The compressibility or compliance K.

(ix) The mass flow gain factor M.

Then if

$$Q = -2\cot\gamma + 2\phi/\sin^2\gamma - 2i\omega\tau(1-\epsilon)/\sin^2\gamma - 2(1-\epsilon)F$$

it transpires that

$$ZP_{11} = ZB_{11} + QZP_{21}, \tag{35}$$

$$ZP_{12} = \lambda(1-\alpha_0)ZB_{12} + Q(1+ZB_{22}) - 2\lambda(1+ZP_{11}), \tag{36}$$

$$ZP_{21} = ZB_{21}/\lambda(1-\alpha_0), \tag{37}$$

$$ZP_{22} = ZB_{22} - 2ZB_{21}/(1-\alpha_0), \tag{38}$$

where, as before, $\lambda = \phi/(1-\alpha_0)^2\sin^2\gamma$ and the elements of $[ZB]$ are computed from (19)–(22), where, with the above variables,

$$\Omega l_c/u_0 = \omega\epsilon\tau(1-\alpha_0)/\phi, \quad fl_c(1-\alpha_0) = F\epsilon/\lambda(1-\alpha_0). \tag{39}$$

This, then, is the source of the transfer functions described in the next section. Before examining these it is, however, instructive to indicate the low frequency limits of the $[ZP]$ elements. Using the asymptotes (23)–(26), it transpires that for small values of ω, K, α_0 and M

$$ZP_{11} \to K\phi F\epsilon/(1-\alpha_0) + \tfrac{1}{2}i\omega K\tau\epsilon\{2\cot\gamma + (2-\epsilon)F + 2\lambda(1-\alpha_0^2)\}, \tag{40}$$

$$ZP_{12} \to -i\omega(2\tau/\sin^2\gamma) - 2\cot\gamma - 2F, \tag{41}$$

$$ZP_{21} \to -\tfrac{1}{2}i\omega\epsilon\tau K, \tag{42}$$

$$ZP_{22} \to -i\omega\epsilon\tau\{(1-\alpha_0)M/\phi - K\lambda\}. \tag{43}$$

Here the expected inertial and resistive terms appear in ZP_{12}, a compliance $\frac{1}{2}\epsilon\tau K$ appears in Z_{21} and a mass flow gain factor appears in Z_{22} which is a function of M and

K, though the second (or K-dependent) term is usually small compared with the first (or M-dependent) term.

Finally it is important to note that the determinant of $[ZP]+[I]$ is always equal to the determinant of $[ZB]+[I]$ and is therefore also given by D [see (27)].

6. Results

In presenting the results for the theoretical transfer functions, it is simplest to fix some of the nine parameters listed in the last section at representative values and explore the variation in the dynamics with the remaining parameters. Thus we shall restrict our attention to a representative impeller like those investigated experimentally by Ng & Brennen (1978) by choosing a blade angle γ of 9° and a value of τ of 0·45. Furthermore we shall choose to examine the dynamics at a mean operating flow coefficient ϕ of 0·07 and plot the results as functions of non-dimensional frequency up to about 0·5.

It is most suitable to choose the value of the blade-passage resistance parameter F such that the total pump resistance in the absence of cavitation and at low frequencies, $2\cot\gamma+2F$, agrees with the value given in figure 2. This demanded a value of F of about 3.

The experimental data in figure 4 were displayed for various values of the mean cavitation number σ; having fixed ϕ, this is the only remaining variable describing the mean operating state. Both the fractional length of the bubbly region ϵ and the mean void fraction will clearly be functions of σ. A reasonable functional relation for $\alpha_0(\sigma)$ was determined from the experimental data in § 3. However, it was established fairly early on in the calculations that the actual value of α_0 had only a minor effect on the transfer matrices; indeed the effect could readily be neglected if α_0 was only 0·1 or 0·2, and according to (4), α_0 approached such values only when σ was quite close to the breakdown cavitation number. Consequently in most of the data presented α_0 is taken as zero for simplicity.

It was therefore clear that the primary effect of the cavitation arose through the variation of ϵ with σ. Measurements of the extent of the cavitating bubbles from photographs of the cavitating Impeller IV at various σ showed that this functional relation could be approximated by

$$\epsilon = \sigma^*/\sigma, \tag{44}$$

where σ^* was a constant with a value of about 0·02 for Impeller IV. However, for the purposes of more general interpretation the results will be presented with ϵ rather than σ values representing the mean flow cavitation condition.

Finally we must discuss the two remaining parameters in the calculations, K and M. No really satisfactory way to determine practical values of these quantities has yet occurred to us. Thus we have simply regarded these for the present as the two arbitrary parameters in the calculation and explored the dependence of the results on these parameters. (In this regard it should be noted that, though ZP_{12} and ZP_{22} depend on both K and M, ZP_{11} and ZP_{21} depend only on K and not on M.)

Pump transfer matrices $[ZP]$ with $\phi = 0{\cdot}07$, $\gamma = 9°$, $\tau = 0{\cdot}45$, $\alpha_0 = 0$, $F = 3$, $K = 0{\cdot}9$ and $M = 0{\cdot}7$ are presented in figure 5 for $\epsilon = 0{\cdot}2$, 0·4, 0·6 and 0·8. The corresponding values of the determinant D are presented in figure 6. For the purpose of

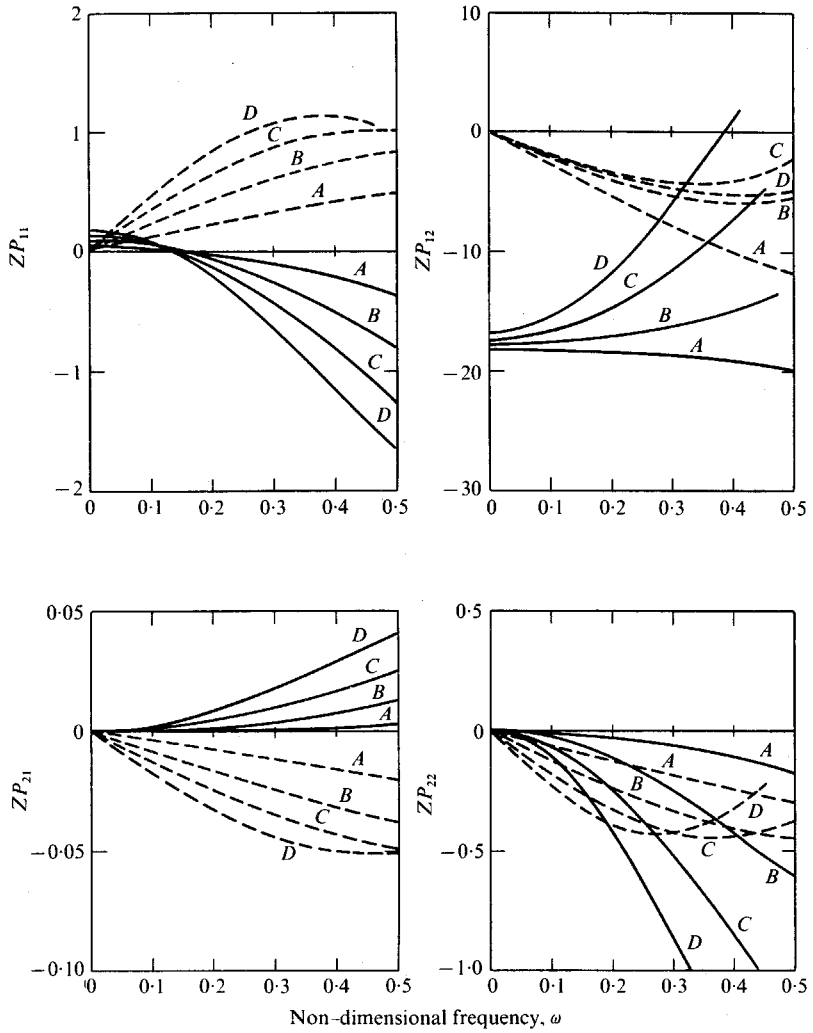

FIGURE 5. Theoretical pump transfer matrices $[ZP]$ for Impeller IV ($\phi = 0{\cdot}07$, $\gamma = 9°$, $\tau = 0{\cdot}45$, $F = 3$) as functions of frequency for $\alpha_0 = 0$, $K = 0{\cdot}9$, $M = 0{\cdot}7$ and the following values of ϵ: (*A*) $\epsilon = 0{\cdot}2$; (*B*) $\epsilon = 0{\cdot}4$; (*C*) $\epsilon = 0{\cdot}6$; (*D*) $\epsilon = 0{\cdot}8$. These correspond to increasingly extensive cavitation or regions of bubbly flow in the blade passage. The real and imaginary parts are represented by solid and dashed lines respectively.

tracing the origin of the $[ZP]$ elements the corresponding bubbly blade-passage region transfer functions $[ZB]$ are displayed in figure 7 for $\epsilon = 0{\cdot}4$ and $0{\cdot}8$. It can be seen by comparing figures 5 and 7 and by examining (35)–(38) that apart from the multiplicative factor λ in ZP_{21} most of the important dynamics in the elements ZP_{11}, ZP_{21} and ZP_{22} are carried straight through from ZB_{11}, ZB_{21} and ZB_{22} and are therefore derived primarily from the dynamic response of the bubbly flow. The impedance element ZP_{12} is primarily the result of the addition of λZB_{12} and the impedance Q of the rest of the blade-passage flow.

It can be seen by comparing figures 2 and 5 that most of the important trends in the data are also manifest by the bubbly flow model. Computations with other choices

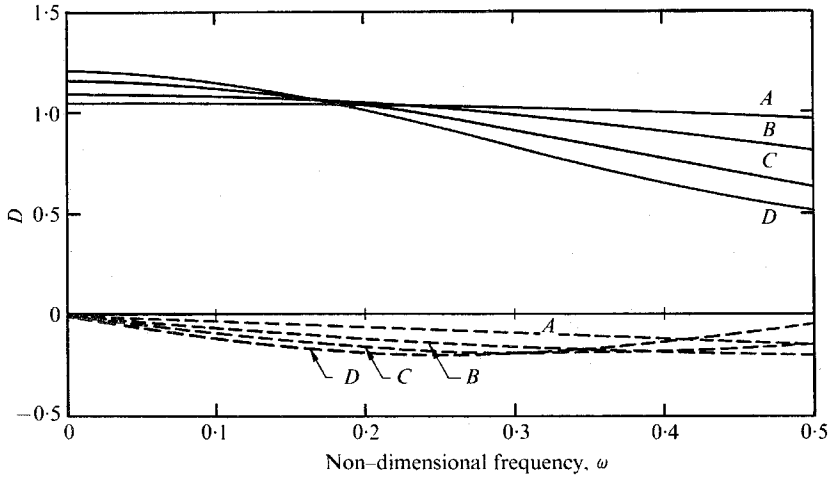

FIGURE 6. The determinants D for the pump matrices in figure 5.

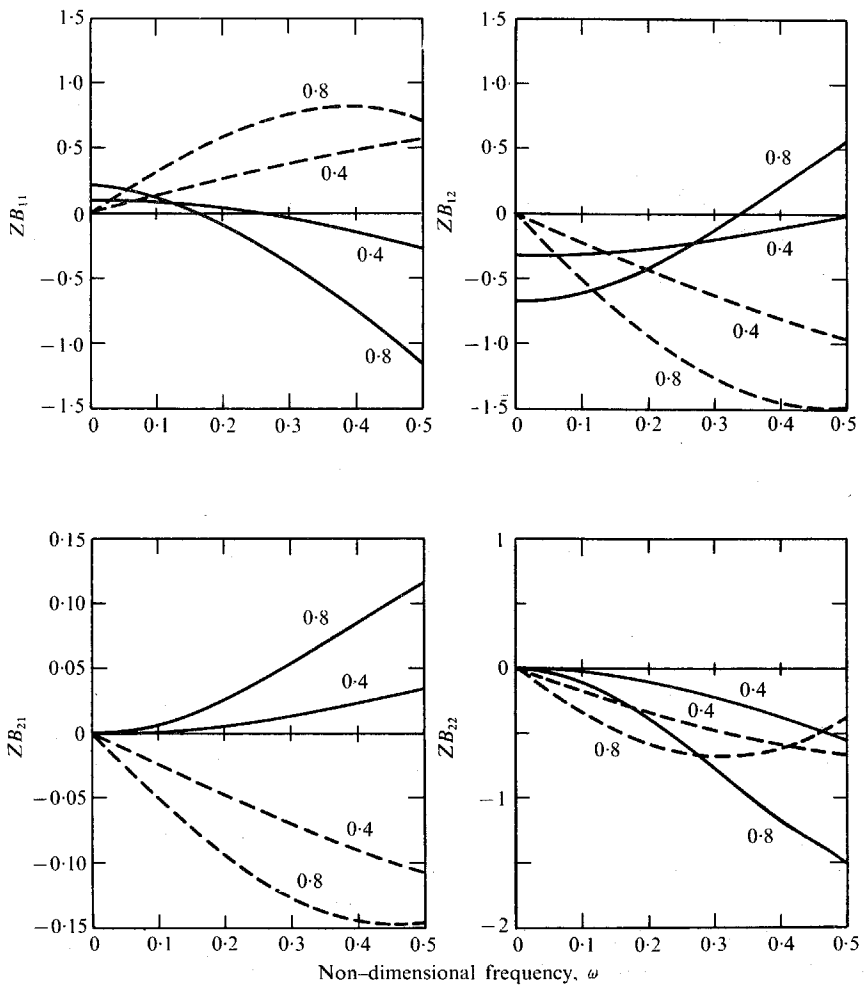

FIGURE 7. The bubbly region transfer matrices $[ZB]$ which correspond to the pump transfer matrices in figure 5. Only the results for $\epsilon = 0{\cdot}4$ and $0{\cdot}8$ are shown.

for K and M indicated that the qualitative trends were the same over a fairly wide range of K and M; however, we have presented the data for $K = 0{\cdot}9$ and $M = 0{\cdot}7$ because values of this order also appeared to yield fair quantitative agreement with the data for Impeller IV (figure 2). In examining the comparison, starting with the impedance ZP_{12}, we should not, of course, expect to reproduce the frequency-dependent behaviour of the resistance and inertia in non-cavitating flow as typified by the curves A in figure 2; a more complex model of the flow without bubbles would be required to do this. However, it is clear that we have reproduced the trends (i) for the resistance at higher frequencies to decrease with increasing cavitation (increasing ϵ) and (ii) for the inertia first to decrease and then increase with increasing cavitation. With regard to this second point we digress briefly to discuss the effect on the computed results of small but non-zero α_0; this is typified by figure 8, which compares the results for $\alpha_0 = 0$ and $\alpha_0 = 0{\cdot}1$ for $\epsilon = 0{\cdot}6$. The earlier statement of the relative insensitivity to α_0 is justified by figure 8. Perhaps the most significant effect of non-zero α_0 is, however, an increase in the inertia. Since values of α_0 of the order of $0{\cdot}1$ or $0{\cdot}2$ would in practice occur only at large ϵ, this would magnify the increase of the inertia with ϵ at large ϵ. The initial decrease and subsequent increase of the inertia with increasing cavitation for all but the highest frequencies is clearly manifest in the experimental data in figure 2.

Turning to ZP_{11}, it would appear that the model is in satisfactory agreement with the data with the exception of the data line E for the real part of ZP_{11} in figure 2, which has a much larger positive value at low frequencies than the corresponding theoretical calculation (e.g. line D in figure 5). The data line E is *not* just an odd data point; other transfer matrices measured at very low cavitation numbers yielded similar large positive intercepts on the $\omega = 0$ axis. The reason for this is not clear at present. (It should however be recalled that Ng & Brennen (1978) pointed out that the measurements at these very low cavitation numbers may include significant nonlinear effects.) As mentioned previously, the model values of ZP_{11} (and ZP_{21}) are independent of M and depend only on K. In this respect it is encouraging to note that during analysis of the dynamics of liquid-oxygen pumps for space vehicles Wagner (1971; see also Rubin, Wagner & Payne 1973) found that the 'pressure gain' (which we interpret somewhat arbitrarily as the real part of ZP_{11}) was proportional to the 'compliance' (or imaginary part of ZP_{21} divided by $-i\omega$). It can be seen from (40) and (42) that at low frequencies this is indeed the case in the present model; the factor of proportionality is equal to $2\phi F/\tau$ for small α_0.

The comparison of experiment and theory for the remaining elements, ZP_{21} and ZP_{22}, requires little discussion. Since the experimental data for these quantities are a little more scattered than for ZP_{11} or ZP_{12} the agreement would appear to be as good as could be expected. The imaginary parts of ZP_{21} and ZP_{22} manifest 'compliances' and 'mass flow gain factors' which increase as the extent of cavitation increases, while the trends in the real parts are consistent with the experimental observations.

The theoretical determinants D corresponding to figure 5 are presented in figure 6 and indicate trends similar to those of the data in figure 3 with increasing cavitation. The importance of this determinant has been stressed in a recent paper (Brennen 1978); the fact that $|D| \neq 1$ in the cavitating cases implies a dynamic element which is behaving actively rather than passively. Both figures show the deviation from a dynamical passive system as σ is decreased (ϵ increased). The discrepancy in the real

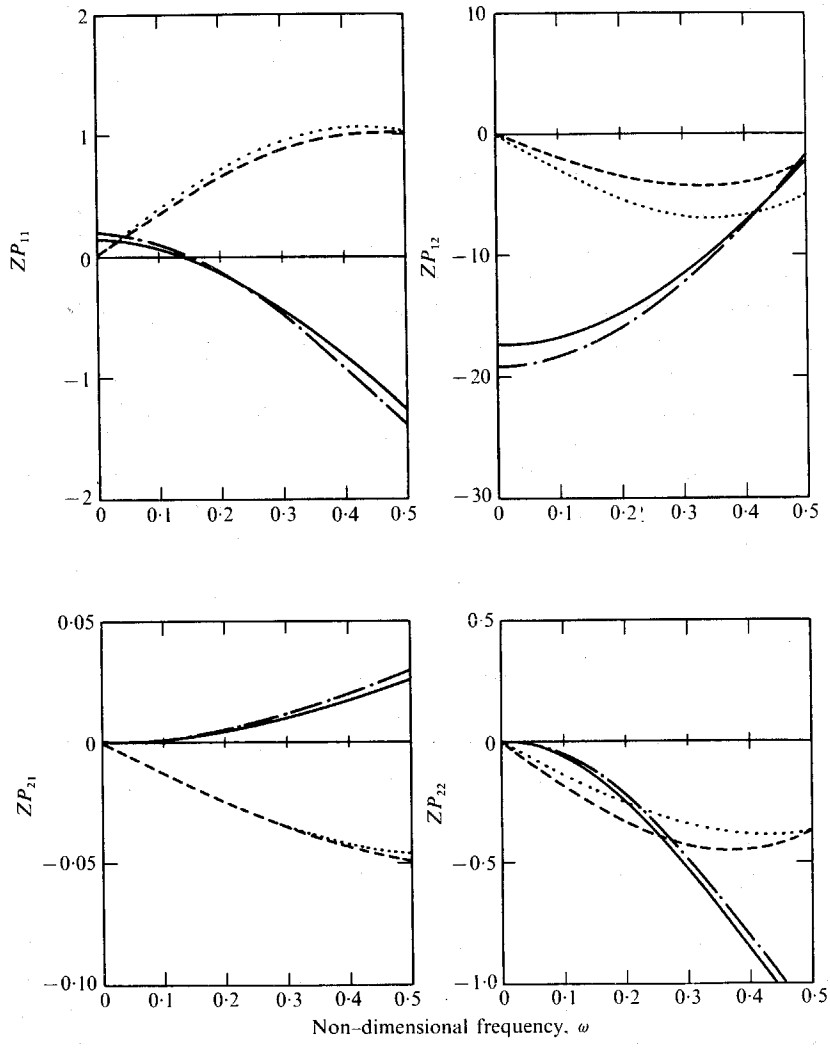

FIGURE 8. The effect of non-zero α_0 on the theoretical pump transfer matrices in figure 5. The solid and dashed lines reproduce the $\epsilon = 0{\cdot}6$ data in figure 5 for which $\alpha_0 = 0$. The dot–dash and dotted lines are respectively the real and imaginary parts of the elements for $\alpha_0 = 0{\cdot}1$.

parts of ZP_{11} at low frequencies manifests itself again in larger values for the real part of D in the data than are forthcoming in the model; the trend is correct but the magnitudes are not in agreement. It should be noted that the deviation of D from unity is primarily a function of the parameter M [see (27)]; in fact, without this oscillatory production rate of bubbles at the leading edge, $|D|$ would always be unity. It is probable that this deviation from passivity is responsible for the pump-induced hydraulic system resonances known as auto-oscillations experienced with many cavitating inducers (see, for example, Sack & Nottage 1965; Young, Murphy & Reddecliff 1972; Natanzon *et al.* 1974; Kamijyo 1975).

7. Concluding remarks

The purpose of this paper has been to explore some of the possible dynamic mechanisms manifest in the measurements of the dynamic transfer matrices of cavitating pumps made by Ng & Brennen (1978). Though the bubbly blade-passage flow model which has been presented here appears to go a long way towards explaining the dynamic characteristics manifest in the experiments, there do remain some questions which seem to need further experimental and theoretical attention. The primary building blocks for the model are the two kinds of dynamic disturbance created in the bubbly blade-passage flow, namely those due to the oscillation in the void fraction caused by the fluctuating production of bubbles at the leading edge (characterized by the parameter M) and those due to the compliance K of the bubbles to the local oscillatory pressure. Indeed, it would not seem unreasonable to suggest that almost any unsteady two-phase flow will in practice exhibit both kinds of wave, the former kinematic and the latter dynamic. In the present context the principal difficulty lies in evaluating the parameter M and the compliance K for a cavitating cascade; the latter is more amenable to theoretical evaluation (e.g. Brennen 1973) but the former requires further attention. The present model is also rather crude in that it treats a flow which is smeared out or averaged laterally across the blade passage and also neglects mean pressure and velocity gradients along the passage. Clearly it is possible to improve the model in these respects though at a cost of considerable algebraic complexity. Prior to implementing such sophistication it would seem wise to carry out further experimental investigations to examine, for example, the propagation of the oscillatory pressure along the blade passage.

The author is very grateful to Professor Allan Acosta for discussions on the subject matter. This work was supported by the National Science Foundation under Research Grant ENG 76-11225 and by NASA George Marshall Space Flight Center under Contract NAS 8-28046.

REFERENCES

Anderson, D. A., Blade, R. J. & Stevens, W. 1971 Response of a radial-bladed centrifugal pump to sinusoidal disturbances for non-cavitating flow. *N.A.S.A. Tech. Note* D-6556.

Brennen, C. 1973 The dynamic behavior and compliance of a stream of cavitating bubbles. *Trans. A.S.M.E., J. Fluids Engng* **95**, 533–542.

Brennen, C. 1978 On the unsteady, dynamic response of phase changes in hydraulic systems. *Proc. Int. Sem., Int. Cen. Heat Mass Transfer, Dubrovnik.* Washington: Hemisphere.

Brennen, C. & Acosta, A. J. 1973 Theoretical, quasi-static analysis of cavitation compliance in turbopumps. *J. Spacecraft Rockets* **10**, 175–180.

Brennen, C. & Acosta, A. J. 1976 The dynamic transfer function for a cavitating inducer. *Trans. A.S.M.E., J. Fluids Engng* **98**, 182–191.

Fanelli, M. 1972 Further considerations on the dynamic behavior of hydraulic turbomachinery. *Water Power*, June 1972, pp. 208–222.

Farrel, E. C. & Fenwick, J. R. 1973 POGO instabilities suppression evaluation. *N.A.S.A. Rep.* CR-134500.

Kamijyo, K., Suzuki, A., Shimura, T., Hashimoto, R., Watanabe, M., Watanabe, Y., Iwabuchi, T. & Mori, Y. 1975 Experimental investigation of small, high-speed, high-head liquid oxygen pump. *Nat. Aerospace Lab. Japan Rep.* TR–415.

NATANZON, M. S., BL'TSEV, N. I., BAZHANOV, V. V. & LEYDERVARGER, M. R. 1974 Experimental investigation of cavitation-induced oscillations of helical inducers. *Fluid Mech., Sov. Res.* **3**, 38–45.

NG, S. L. 1976 Dynamic response of cavitating turbomachines. Ph.D. thesis, California Institute of Technology, Pasadena. (See also *Div. Engng Appl. Sci., Caltech, Rep.* E184.1.)

NG, S. L. & BRENNEN, C. 1978 Experiments on the dynamic behavior of cavitating pumps. *Trans. A.S.M.E., J. Fluids Engng* **100**, 166–176.

NG, S. L., BRENNEN, C. & ACOSTA, A. J. 1976 The dynamics of cavitating inducer pumps. *Proc. Int. Conf. Two Phase Flow Cavitation, Int. Assoc. Hyd. Res., Grenoble*, pp. 383–398.

RUBIN, S. 1966 Longitudinal instability of liquid rockets due to propulsion feedback (POGO). *J. Spacecraft Rockets* **3**, 1188–1195.

RUBIN, S., WAGNER, R. G. & PAYNE, J. G. 1973 POGO suppression on space shuttle – early studies. *N.A.S.A. Rep.* CR-2210.

RUNDSTADLER, P. W. 1976 Review and analysis of state-of-the-art of multiphase pump technology. *Electric Power Res. Inst., Palo Alto, Calif., Rep.* NP-159.

SACK, L. E. & NOTTAGE, H. B. 1965 System oscillations associated with cavitating inducers. *J. Basic Engng* D **87**, 917–925.

STRIPLING, L. B. & ACOSTA, A. J. 1962 Cavitation in turbopumps – Part I. *J. Basic Engng* D **84**, 326–338.

VAAGE, R. D., FIDLER, L. E. & ZEHNLE, R. A. 1972 Investigation of characteristics of feed system instabilities. *Martin Marietta Corp., Denver, Colorado, Final Rep.* MCR-72-107.

WAGNER, R. G. 1971 Tital II engine transfer function test results. *Aerospace Corp., El Segundo, Calif., Rep.* TOR-0059 (G471)-9.

YOUNG, W. E., MURPHY, R. & REDDECLIFF, J. M. 1972 Study of cavitating inducer instabilities. *Pratt Whitney Aircraft, Florida, R. & D. Center Rep.* PWA FR-5131.

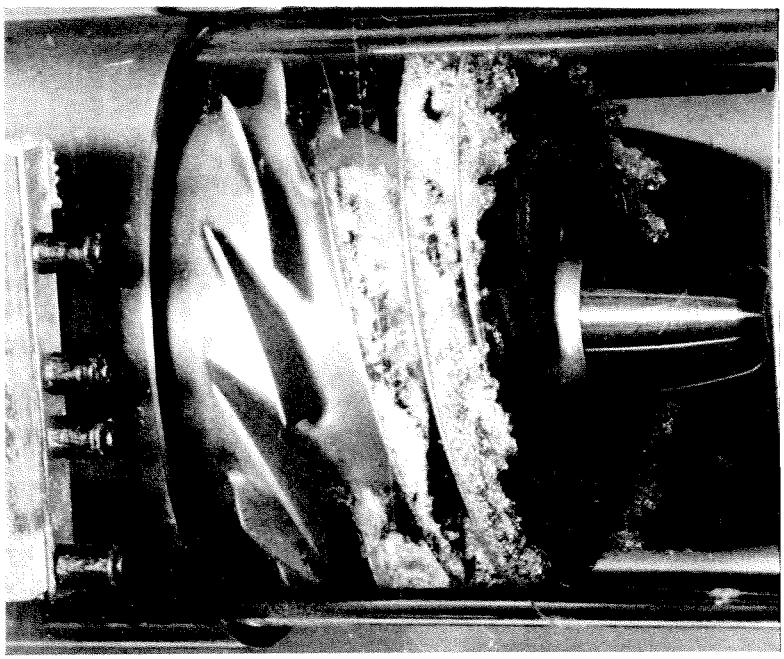

FIGURE 1. A high-speed photograph of the cavitation in Impeller IV taken during the experiments of Ng & Brennen (1978) under conditions of extensive cavitation ($\sigma \cong 0{\cdot}024$). The flow is from right to left.